Soil Shearing during Earthquake Surface Fault Rupture

N.K. Oettle & J.D. Bray
University of California, Berkeley, USA

SUMMARY:
Several recent earthquakes have resulted in significant damage to structures as a result of surface fault rupture. Although a number of researchers have studied the earthquake surface fault rupture problem, a thorough examination of the predominant modes of soil shearing during the fault rupture process has yet to be characterized comprehensively. In this study, the authors have conducted a series of numerical analyses to analyze the mechanics of dip-slip surface fault rupture. The numerical results demonstrate that the soil rupture process can be divided into two important mechanical stages applicable to both reverse and normal fault ruptures through soil: (1) broad deformation before strain localization occurs; and (2) more localized deformation after shear band formation. Stress paths in the rupture zone were found to be approximately analogous to plane-strain extension (loading) and plane-strain compression (unloading) element tests for reverse and normal faults, respectively.

Keywords: constitutive model, earthquake, numerical analysis, soil shear, surface fault rupture

1. INTRODUCTION

Recent earthquakes have provided numerous examples of the devastating effects of earthquake surface fault rupture on the built environment (e.g., 1999 Kocaeli Earthquake, 1999 Chi-Chi Earthquake, and 2008 Wenchuan Earthquake). Along with the often spectacular observations of damage (e.g., Kelson et al., 2001), examples of satisfactory performance of structures have also been observed (e.g., Lazarte et al., 1994). These examples of satisfactory performance indicate that similar to other forms of ground failure, effective design strategies can be developed to address the hazards associated with surface fault rupture (Bray, 2001). A rational design and mitigation framework for addressing the surface fault rupture hazard is required.

A key to developing a rational design framework is to develop an understanding of the mechanics involved in the surface fault rupture process. Several researchers have completed important work in this area (e.g., Bray et al. 1994a, Johansson and Konagai 2005, and Anastasopoulos et al. 2008). Researchers who have worked on the numerical modeling of earthquake surface fault rupture have concluded that there are several important aspects of soil response that needed to be modeled for the earthquake surface fault rupture process. These key features necessary for properly modeling surface fault rupture are: stress-strain nonlinearity (Bray et al., 1994b), soil failure strain (Bray et al., 1994b), the undrained response (Johansson and Konagai 2005), and strain softening (Anastasopoulos et al., 2007). This study seeks to expand upon these previous studies with a focus on investigating the fundamental response of soil during shearing as a result of dip-slip fault displacements.

2. NUMERICAL MODEL

The surface fault rupture process is analyzed using the two-dimensional finite-difference computer program FLAC (Itasca, 2011) in the plane-strain mode. Large-strain calculations and rezoning logic available in FLAC are used to enhance the numerical model and allow a fine mesh coupled with large bedrock displacements.

The selected constitutive model is based upon the widely used UBCSAND elasto–plastic, effective-stress constitutive model (Byrne et al., 2004). Modifications are made to the UBCSAND model (version dated 26 July 2009 from Prof. Peter M. Byrne, personal communication) for the purposes of this study. The primary modification is the incorporation of post-peak strain softening. Strain softening is modeled by linearly decreasing the yield surface to the critical state stress ratio over a specified shear strain after the peak stress ratio is reached. Modeling strain softening creates a mesh-dependent solution in which strains measured after peak stress are proportional to the element size since the shear band over which relative slip occurs is of a fixed width. This limitation was partially addressed using the same methodology as Anastasopoulos et al. (2007) which sets the strain over which an element that fully softens as being proportional to the size of the element based on an assumed displacement required to fully soften the shear band. Other modifications include a friction angle dependence on the log of confining stress and changes to the cycle-logic of UBCSAND to accommodate the aforementioned changes. Representative element test results for this modified version of UBCSAND are presented in Figure 1.

Earthquake surface fault rupture is analyzed for the case of a dry sand deposit that overlies rigid bedrock. A single reverse or normal fault rupture in the underlying bedrock is analyzed by applying displacement at the base of the sand deposit and the appropriate lateral displacements along the model boundaries on the hanging wall and applying fixity on the footwall boundaries. The bedrock displacement is applied monotonically and pseudo-statically. These conditions are similar to or the same as those used by previous researchers (e.g., Bray et al. 1994b).

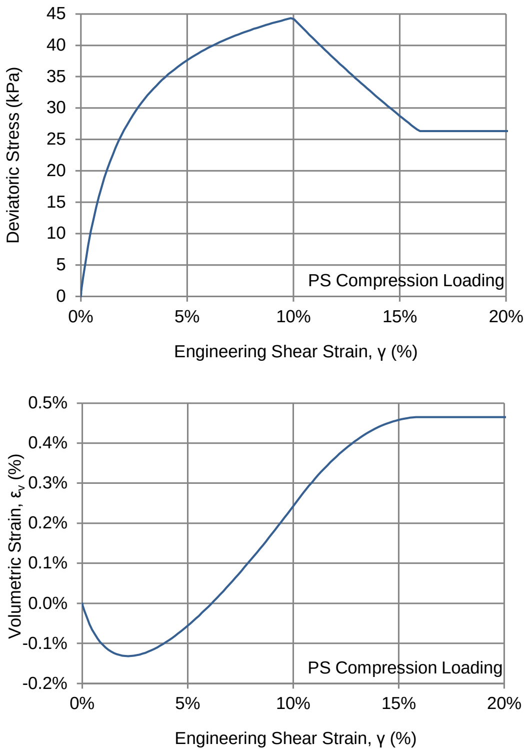

Figure 1. Modified-UBCSAND element test results for plane strain compression loading ($N_{1,60}$=22, K_0=0.45)

3. SOIL MODEL RESPONSE EVALUATION AND CALIBRATION

The capabilities of the FLAC-based, modified-UBCSAND numerical simulations to capture the key characteristics of earthquake surface fault rupture propagation through soil were evaluated using the results of a comprehensive series of geotechnical centrifuge test results reported in Bransby et al. (2008a and b) with additional information provided by Profs. G. Gazetas and I. Anastasopoulos (personal communication). The centrifuge experiments were back-analyzed with the numerical simulations described herein, and the results of the simulations were compared with those of the carefully performed and documented physical model experiments to evaluate the robustness of the analytical procedures.

Preliminary UBCSAND model parameters were developed based on recommendations provided in Beaty and Byrne (2011). A parameter sensitivity test was conducted to evaluate the model response to reasonable changes in the value of key parameters. The physically significant parameters were limited to a range typical of sand (e.g., the critical state, effective friction angle (ϕ_{cv}) was kept between 30° and 33°).

Two new parameters are introduced in a modified version of the UBCSAND soil constitutive model as part of this study to better capture soil response and failure during earthquake fault rupture propagation. Firstly, the change in the soil's peak friction angle as a function of confining stress is modeled through the parameter $\Delta\phi$ as defined in Duncan and Wright (2005). This parameter captures the decrease in the soil's effective-stress friction angle for a log cycle increase in effective confining stress. The parameter $\Delta\phi$ is set to 4° in this study. Secondly, the shear strain required to decrease the yield surface from peak to critical state (strain softening) is set to 6% when the mesh size was approximately 0.2 m for the analysis of soil deposits at prototype scale. When back-analyzing centrifuge test results, the shear strain required to decrease the yield surface from peak to critical state was considerably larger due to the linear scaling of particle size with centrifuge *g* level. For the back-analyses of centrifuge tests, a mesh size of 0.4 m was used, because the shear band thickness was measured to be approximately 0.4 m at prototype scale during the centrifuge testing in Bransby et al. (2008a). The relative displacement necessary to fully soften the shear band is assumed to be 100 times the sand particle's median grain size (Bransby et al., 2008a). With a roughly 0.3 mm-sized sand particle at model scale (i.e., the actual size of the model sand), the size of the sand particle is 34 mm at prototype scale if the centrifuge *g* level is 115 (i.e., 115*0.3 mm). In contrast, at prototype scale, the shear band size is expected to be less than a centimeter for a fine sand with median particle size of about 0.1 mm. This is too small to model with a single element, so a 0.2 m-wide element is selected for this case, which leads to full softening of the shear band at a shear strain of approximately 6%.

In general, good agreement between the centrifuge test results and the calibrated numerical model were obtained. A representative deformed mesh is presented in Figure 2 and compared to centrifuge test results. The numerical model matched the curvature of the shear band and the slope and shape of the ground surface. The deformation of the soil surface of the same centrifuge test is compared to that calculated with the numerical simulations in Figure 3. The numerical model matched the location of the outcropping shear band as well as the slope of the ground surface near the outcrop. The numerical model calculated ground deformation in excess of what the centrifuge recorded just to the footwall side of the shear band, but matched fairly well the surface movement on the hanging-wall side.

In the simulations discussed in this paper, the values of the original soil UBCSAND model parameters employed in these simulations were identical to those recommended in Beaty and Byrne (2011), except that R_f was fixed to 0.95 to obtain a relatively high level of nonlinearity in the soil's stress-strain response, and the hfac1 parameter (a factor applied to the plastic modulus) was decreased to model accurately the soil's failure strain. The UBCSAND model with hfac1=1.0 and $(N_1)_{60}$=22 results in a plane-strain compression (loading) failure shear strain of approximately 0.3%, which is unreasonably low. The importance of capturing the failure strain parameter in surface fault rupture problems was emphasized in Bray et al. (1994b). Calibrated values of hfac1 were developed by analyzing incremental surface deformation patterns. This approach provided greater sensitivity to changes in the soil model parameters than by just examining the total surface deformation. Incremental surface displacement patterns (discussed later) underwent recognizable changes in their form which allowed for easier comparison between centrifuge and numerical results. An hfac1 value of 0.025 was used to provide the best match of the numerical results to the experimental results for this problem. A summary of the experimental conditions and the calibrated soil model parameters are presented in Tables 3.1 and 3.2, respectively.

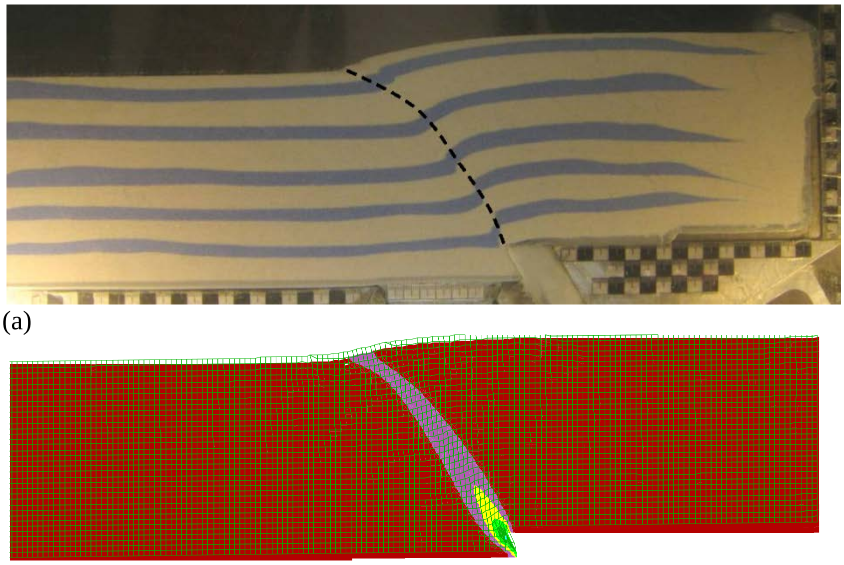

(a)

(b)

Figure 2. Validation of numerical model with centrifuge test 28 from Bransby et al. (2008b): (a) picture of centrifuge experiment; (b) deformed mesh and shear strain contours for numerical model (reverse fault, 60° dip, 15-m soil, $N_{1,60}$=22, K_0=0.45)

4. RESULTS

4.1 Stress Regime

4.1.1. Reverse Faults

Principal stress orientations were recorded for reverse ruptures with the test conditions and model parameters presented in Table 4.1. A representative stress pattern is presented in Figure 5. It was determined that for normally consolidated, at-rest soil deposits with K_o = 0.45, the principal stresses are rotated over a wide area, forming an “arch of stress” over the bedrock fault. In situ K_o stress conditions are maintained away from the bedrock dislocation. In the “arch of stress” zone , high shear stresses develop in the soil deposit as a result of the bedrock fault rupture. A shear band is formed eventually in the center of the zone of high shear stress. This shear band was often found to curve downward slightly for reverse faults (i.e., decrease in dip near the ground surface). The ground surface deformation response was highest at the outcropping location of this shear band and decreased away from the shear band.

Table 3.1. Test conditions for validation

CONDITION	VALUE
Style of faulting	Reverse and normal, 60° dip
Position of rupture	Varies for each centrifuge test
Height of soil	Varies for each centrifuge test
Width of model	Varies for each centrifuge test
Element width	0.4 m
Applied boundary velocity (in direction of movement)	1e-6 m/s
K_o, at-rest earth pressure coefficient	0.45

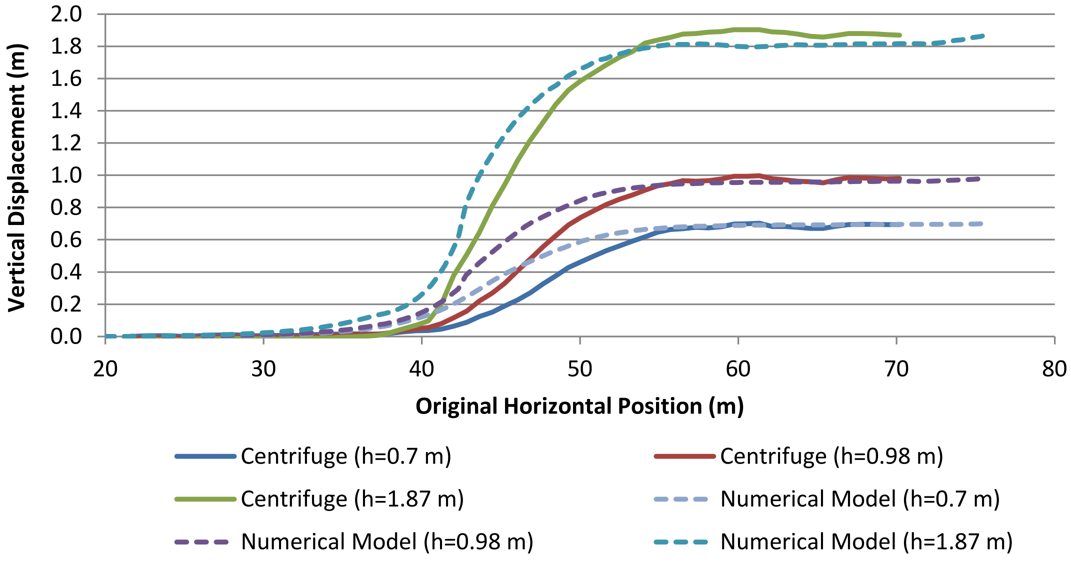

Figure 3. Validation of numerical model with centrifuge test 28 from Bransby et al. (2008b): profile of vertical displacement recorded across the fault near the ground surface

Table 3.2. Model parameters for validation

PARAMETER	VALUE
Density	1.6 kg/m^3
$(N_1)_{60}$, corrected SPT blow count	Varies with reported D_r
ϕ_{cv}, critical-state effective-stress friction angle	33°
Atmospheric pressure	100 kPa
m_e, elastic shear modulus stress dependence	0.5
n_e, elastic bulk modulus stress dependence	0.5
n_p, plastic shear modulus stress dependence	0.4
Hfac1, modification to plastic modulus	0.025
Hfac2, modification to plastic modulus	1.0
Anisotropy factor	1.0
$\Delta\phi$, change in peak effective-stress friction angle	4°
G_{max}, elastic shear modulus	$21.7*20*(N_1)_{60}^{0.333}$
K, elastic bulk modulus	$G_{max}*0.7$
G_p, initial plastic shear modulus	$0.003*G_{max}*(N_1)_{60}^2 + 100$
ϕ_0, peak effective-stress friction angle	$\phi_{CV} + (N_1)_{60}/10 + \max(0,((N_1)_{60}-15)/5)$
R_f, hyperbolic stiffness parameter	0.95
Post-peak shear strain to critical state	8.57

Table 4.1. Test conditions and model parameters

CONDITION	VALUE
Style of faulting	Reverse and normal, 60° dip
Position of rupture	30 m from footwall boundary
Height of soil	15 m
Width of model	50 m (reverse), 55 m (normal)
Element width	0.2 m
$(N_1)_{60}$, corrected SPT blow count	22 ($D_r \approx 60\%$) or 34 ($D_r \approx 75\%$)
Post-peak shear strain to critical state	0.06
Other parameters	Same as in Tables 3.1 and 3.2

For an element in the center of the soil deposit in the location of the developing shear zone, the minor principal stress is increased until a near isotropic stress state is reached. Continued shearing causes the horizontal stress to exceed the vertical stress in the center of this region. As this occurs, the minor principal stress decreases and the major principal stress increases until a failure state is reached. This stress path is presented in Figure 5.

The stress path of the soil in the location of the developing shear band (i.e., near the middle of the "arch of stress" zone; noted as Element A') is most similar to the stress path of a plane-strain extension (loading) laboratory test (as defined in Wood, 1990). However, the stress path also contains a component of minor principal stress reduction, unlike a typical plane-strain extension (loading) test. The stress path shown in Figure 5 for the case of a reverse fault is also somewhat analogous to Rankine passive earth pressure conditions. It should take relatively more bedrock fault displacement to mobilize fully the Rankine passive condition than the Rankine active condition.

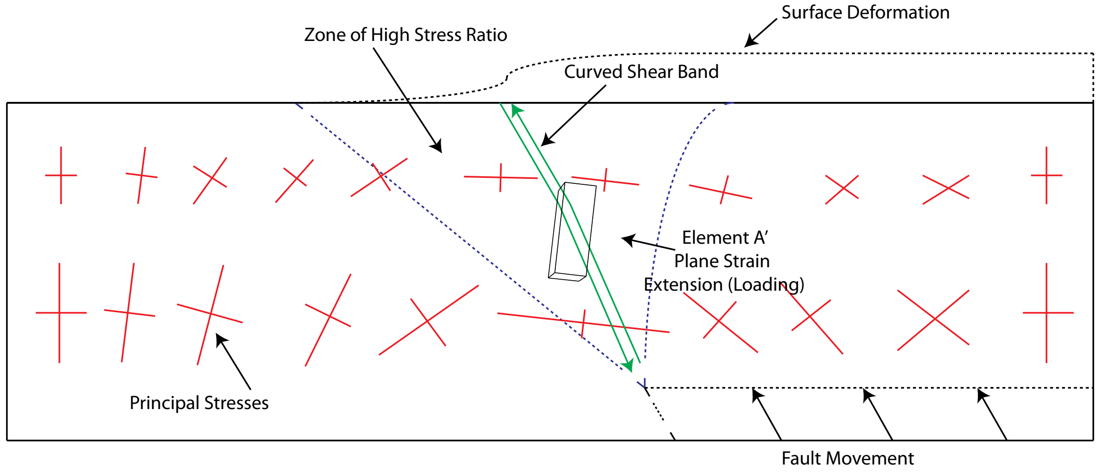

Figure 4. Schematic of a reverse fault rupture through dry sand (60° dip, 15-m soil, 0.7 m of vertical fault movement, $N_{1,60}$=34, K_0=0.45, unfaulted soil)

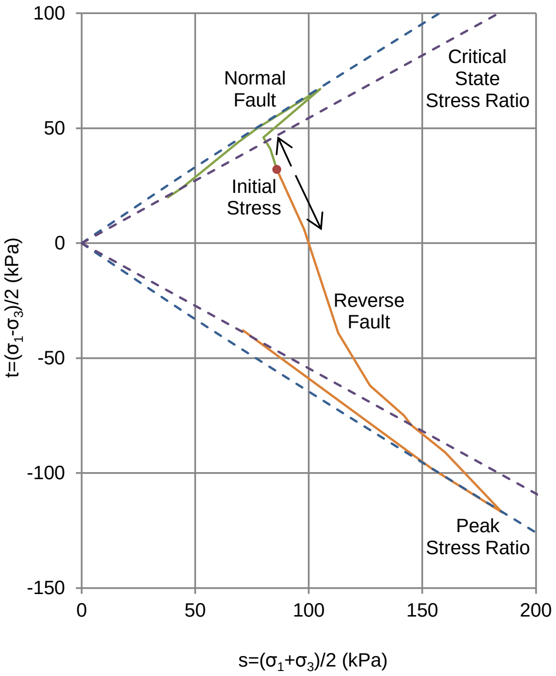

Figure 5. Stress paths for reverse and normal fault ruptures where shear stress is taken as negative when the major principal stress is more horizontal than vertical (Element A' in Figure 4 and Element B' in Figure 6)

4.1.2. Normal Faults

In normal faults, principal stresses rotate in a relatively small zone near the rupture. The major principal stress in the rupture zone "bends over" slightly to accommodate shear along the rupture plane. Unlike reverse faults, low-angle dipping normal faults generate a second zone of high stress ratio antithetic to the primary rupture. Between the two zones of high stress ratio, a graben is formed to kinematically accommodate curvature in the primary normal fault shear zone. Away from the fault, K_o stress conditions are maintained. A representative stress pattern is presented in Figure 6.

The stress path in the shear zone during normal faulting can be represented approximately by the plane-strain compression (unloading) shearing mode. The major principal stress remained almost constant while the minor principal stress decreased until failure. The major principal stress rotated slightly, but remained in a predominantly vertical direction. This stress path is presented in Figure 5. The stress path shown in this figure for the case of a normal fault is also somewhat analogous to Rankine active earth pressure conditions, which can be contrasted to the case of the reverse fault movement discussed previously, which is analogous to the Rankine passive condition.

4.2 Surface Deformation

For unfaulted soils overlying a bedrock fault, wherein the soils have been normally consolidated under one-dimensional loading where the highest stress is vertical, deformation at the ground surface is initially distributed over a large zone. The width of this zone is roughly proportional to the thickness of the underlying soil. As relative displacement of the bedrock fault increases, peak stresses are developed eventually in the soil from the bedrock to the ground surface. The bedrock displacement required for peak stress development along the full height of soil is presented in Bray et al. (1994b). If the soil is dilative, further fault displacement creates a shear band and eventually strain softens to critical state.

During the processing of developing a shear band, surface deformation becomes increasingly localized at the ground surface. A comparison of surface deformation patterns for several 0.3 m increments of bedrock displacement is presented in Figure 7. Most reverse and normal fault ruptures, with sufficient soil dilatancy, will develop a deformation pattern similar to that shown in Figure 7. When analyzing centrifuge data or numerical data, the surface deformation shape, whether broad or localized, is diagnostic of the extent of shear band development.

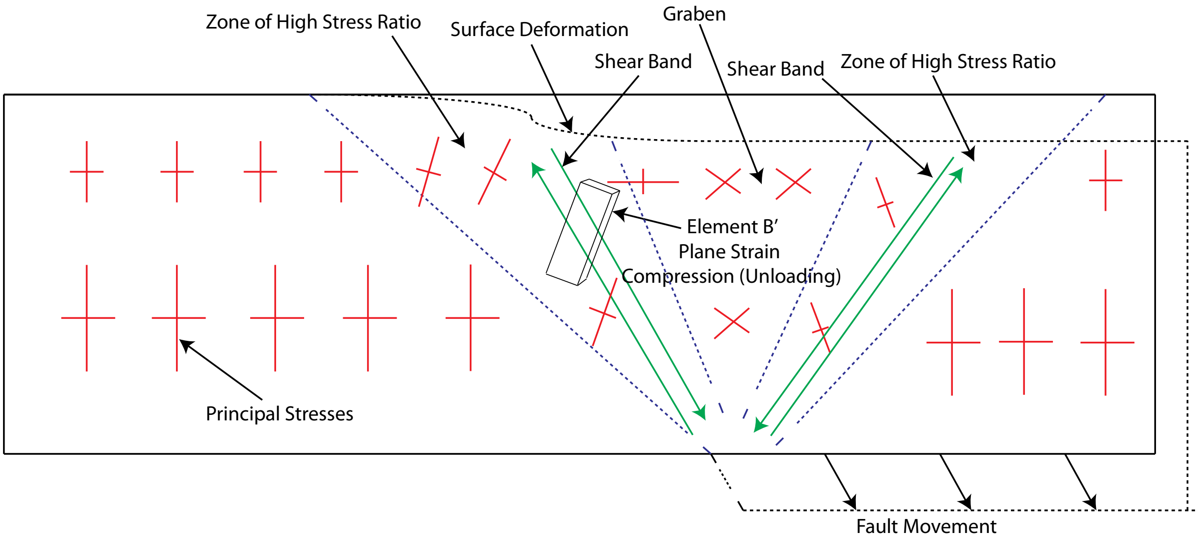

Figure 6. Schematic of a normal fault rupture through dry sand (60° dip, 15-m soil, 0.5 m of vertical fault movement, $N_{1,60}$=34, K_0=0.45, unfaulted soil)

Multiple earthquakes occurring in sequence could develop patterns of stress state and shear band development similar to those depicted in Figures 4 and 6 for reverse and normal fault displacements, respectively. Depending on the effects of stress relaxation, repeated rupturing of the bedrock fault would lead to a more localized response. For example, if the soil stress state and response shown for the increment of bedrock displacement of 2.1-2.4 m that is shown in Figure 7 were considered as the initial conditions for a subsequent earthquake fault movement on the order of 0.3 m of offset, the previously ruptured soil would likely respond very differently than for the case of a fault rupture through unfaulted soil shown in Figure 7 for the bedrock displacement of 0-0.3 m. Therefore, the surface deformation pattern will likely be a function of the soil's seismic history and by extension, the age of the soil, depending on how stress relaxation affects the near-surface region.

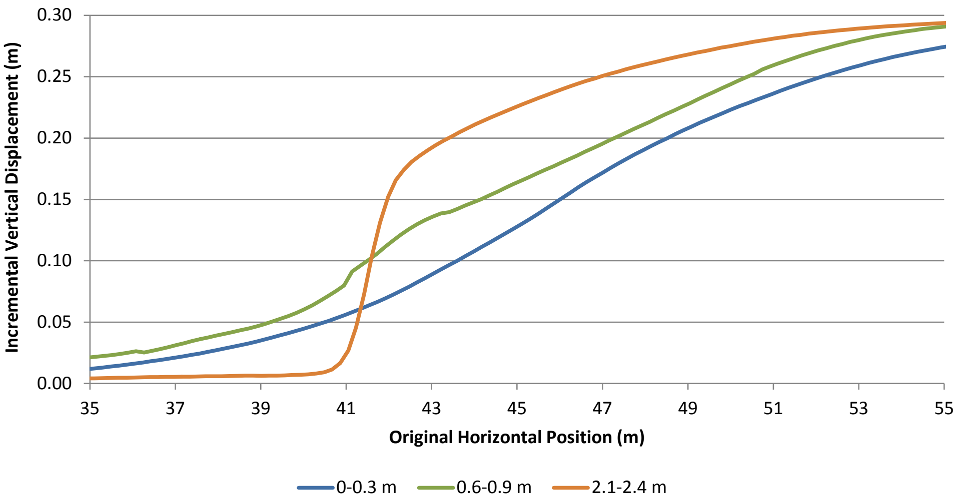

Figure 7. Surface deformation for 0.3 m increments of bedrock displacement (reverse fault, 60° dip, 15-m soil, $N_{1,60}$=22, K_0=0.45)

5. CONCLUSIONS

In this study, calibrated numerical simulations were performed to investigate the mechanical response of earthquake surface fault rupture propagation through soil. The results of these analyses support these conclusions:

- Stress paths and intermediate stresses in the rupture zone are somewhat analogous to plane-strain extension (loading) and plane-strain compression (unloading) element tests for reverse and normal faults, respectively.
- The soil rupture process can be divided into two important mechanical stages applicable to both reverse and normal fault ruptures: (1) broad deformation before strain localization occurs; and (2) more localized deformation after shear band formation. This effect can most readily be seen in plots of incremental surface displacement (e.g., Figure 7) and are diagnostic of the development of shear bands in the faulted soil.
- A previously faulted soil deposit has different initial stress conditions and shear band development compared to a previously unfaulted soil deposit. Thus, it will likely respond differently than previously unfaulted soil deposits. Surface deformation is likely dependent on the soil's seismic history and, by extension, the age of the soil.

ACKNOWLEDGEMENT
Financial support was provided by the National Science Foundation under Grant CMMI-0926473, and this support is gratefully acknowledged. Any opinions, findings, and conclusions or recommendations expressed in this material are those of the authors and do not necessarily reflect the views of the NSF.

REFERENCES

Anastasopoulos, I., Callerio, A., Bransby, M.F., Davies, M.C.R., El Nahas, A., Faccioli, E., Gazetas, G., Masella, A., Paolucci, R., Pecker, A., and Rossignol, E. (2008). Numerical analyses of fault-foundation interaction. *Bulletin of Earthquake Engineering.* **6:4**, 645-675.

Anastasopoulos, I., Gazetas, G., Bransby, M.F., Davies, M.C.R., and El Nahas (2007). Fault Rupture Propagation through Sand: Finite-Element Analysis and Validation through Centrifuge Experiments. *Journal of Geotechnical and Geoenvironmental Engineering.* **133:8**, 943-958.

Bransby, M.F., Davies, M.C.R., and El Nahas, A. (2008a). "Centrifuge modeling of normal fault–foundation interaction." Bulletin of Earthquake Engineering, 6(4), pp. 585–605.

Bransby, M.F., Davies, M.C.R., El Nahas, A., and Nagaoka, S. (2008b). "Centrifuge modeling of reverse fault–foundation interaction." Bulletin of Earthquake Engineering, 6(4), pp. 607–628.

Bray, J.D., Seed, R.B., Cluff, L.S., and Seed, H.B. (1994a). Earthquake Fault Rupture Propagation through Soil. *Journal of Geotechnical Engineering.* **120:3**, 543-561.

Bray, J.D., Seed, R.B., Cluff, L.S., and Seed, H.B. (1994b). Analysis of Earthquake Fault Rupture Propagation through Cohesive Soil. *Journal of Geotechnical Engineering.* **120:3**, 562-580.

Bray, J.D. (2001). Developing Mitigation Measures for the Hazards Associated with Earthquake Surface Fault Rupture. *A Workshop on Seismic Fault-Induced Failures – Possible Remedies for Damage to Urban Facilities.* Research Project 2000 Grant-in-Aid for Scientific Research (No. 12355020), Japan Society for the Promotion of Science, Workshop Leader, Kazuo Konagai, University of Tokyo, Japan: 55-79.

Beaty, M.H., and Byrne, P.M. (2011). "UBCSAND constitutive model version 904aR." *Documentation Report*: UBCSAND Constitutive Model on Itasca UDM Website.

Byrne, P.M., Park, S.S., Beaty, M., Sharp, M.K., Gonzalez, L., and Abdoun, T. (2004). Numerical modeling of liquefaction and comparison with centrifuge tests. *Canadian Geotechnical Journal.* **41:2**, 193-211.

Duncan, J.M. and Wright, S.G. (2005). Soil Strength and Slope Stability. John Wiley & Sons, Inc., Hoboken, NJ.

Itasca (2008). FLAC – Fast Lagrangian Analysis of Continua, Version 6.0. Itasca Consulting Group, Minneapolis, MN.

Johansson, J. and Konagai, K. (2006). Fault induced permanent ground deformation – an experimental comparison of wet and dry soil and implications for buried structures. *Soil Dynamics and Earthquake Engineering.* **26:1**, 45-63.

Kelson, K. and 13 co- authors (2001). Fault-related surface deformation. *Earthquake Spectra.* Special Volume on the Chi-Chi Taiwan Earthquake of September 21, 1999, **17:S1**, 19-36.

Lazarte, C.A, Bray, J.D., Johnson, A.M., and Lemmer, R.E. (1994). Surface Breakage of the 1992 Landers Earthquake and Its Effects on Structures. *Bulletin of the Seismological Society of America.* **84:3**, 547-561.

Wood, D.M. (1990). "Soil behavior and critical state soil mechanics." Cambridge University Press.